Applied Energy 240 (2019) 698–708

Contents lists available at ScienceDirect

Applied Energy

journal homepage: www.elsevier.com/locate/apenergy

Combined ammonia recovery and solid oxide fuel cell use at wastewater treatment plants for energy and greenhouse gas emission improvements

Oliver Grasham[a,b,*], Valerie Dupont[a], Miller Alonso Camargo-Valero[c,d], Pelayo García-Gutiérrez[a], Timothy Cockerill[e]

[a] School of Chemical and Process Engineering, Faculty of Engineering, University of Leeds, Leeds LS2 9JT, United Kingdom
[b] Centre for Doctoral Training Bioenergy, Faculty of Engineering, University of Leeds, Leeds LS2 9JT, United Kingdom
[c] BioResource Systems Research Group, School of Civil Engineering, University of Leeds, Leeds LS2 9JT, United Kingdom
[d] Departamento de Ingeniería Química, Universidad Nacional de Colombia, Campus La Nubia, Manizales, Colombia
[e] Centre for Integrated Energy Research (CIER), Leeds LS2 9JT, United Kingdom

HIGHLIGHTS

- 82% ammonia recovery from wastewater treatment plant digestate liquor.
- Combined ammonia and biomethane fed solid oxide fuel cell modelled.
- Increased renewable electrical power production of 45% compared with conventional system.
- GHG emission reduction of 3.5 kg CO_2e per year for each person served by treatment facility.

GRAPHICAL ABSTRACT

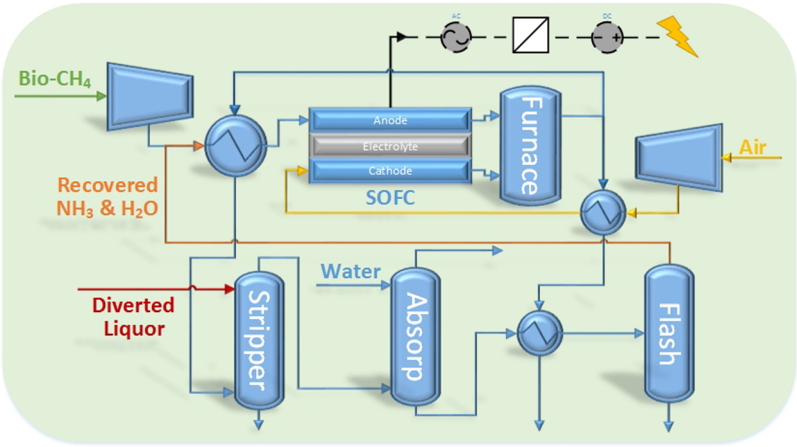

ARTICLE INFO

Keywords:
Ammonia recovery
Wastewater treatment
Fuel Cell
Process modelling
Greenhouse gases

ABSTRACT

Current standard practice at wastewater treatment plants (WWTPs) involves the recycling of digestate liquor, produced from the anaerobic digestion of sludge, back into the treatment process. However, a significant amount of energy is required to enable biological breakdown of ammonia present in the liquor. This biological processing also results in the emission of damaging quantities of greenhouse gases, making diversion of liquor and recovery of ammonia a noteworthy option for improving the sustainability of wastewater treatment. This study presents a novel process which combines ammonia recovery from diverted digestate liquor for use (alongside biomethane) in a solid oxide fuel cell (SOFC) system for implementation at WWTPs. Aspen Plus V.8.8 and numerical steady state models have been developed, using data from a WWTP in West Yorkshire (UK) as a reference facility (750,000p.e.). Aspen Plus simulations demonstrate an ability to recover 82% of ammoniacal nitrogen present in digestate liquor produced at the WWTP. The recovery process uses a series of stripping, absorption and flash separation units where water is recovered alongside ammonia. This facilitates effective internal steam methane reforming in the fuel cell with a molar steam:CH_4 ratio of 2.5. The installation of the process at the WWTP used

* Corresponding author at: School of Chemical and Process Engineering, Faculty of Engineering, University of Leeds, Leeds LS2 9JT, United Kingdom.
E-mail address: ee11og@leeds.ac.uk (O. Grasham).

https://doi.org/10.1016/j.apenergy.2019.02.029
Received 14 August 2018; Received in revised form 29 January 2019; Accepted 6 February 2019

as a case of study has the potential to make significant impacts energetically and environmentally; findings suggest the treatment facility could transform from a net consumer of electricity to a net producer. The SOFC has been demonstrated to run at an electrical efficiency of 48%, with NH_3 contributing 4.6% of its power output. It has also been demonstrated that 3.5 kg CO_2e per person served by the WWTP could be mitigated a year due to a combination of emissions savings by diversion of ammonia from biological processing and lifecycle emissions associated with the lack of reliance on grid electricity.

Nomenclature

A_{cell}	cell active area (m^2)
CHP	combined Heat and Power
CV	cell voltage (V)
D_{eff}	effective diffusivity (m^2/s)
D_{O_2}	oxygen ordinary diffusivity (m^2/s)
E	Nernst voltage potential (V)
E_a	activation energy (J)
E_o	reference voltage (V)
F	Faraday constant (96,485 C mol^{-1})
I	current (A)
j	current density (A m^{-2})
j_l	limiting current densities (A m^{-2})
j_0	exchange current density (A m^{-2})
$\dot{m}_x$	mass flow rate of species x (kg/h)
n	number of participating electrons
n_{act}	activation loss (V)
n_{ohm}	Ohmic loss (V)
n_{conc}	concentration loss (V)
NH3-DEC	ammonia decomposition reaction (R5)
$P_{AC,net}$	net AC system power (kW)
P_{cell}	cell operating pressure (bar)
p.e.	population equivalent
P_{gross}	cell output power (kW)
Q_L	heat loss from cell (kW)
Q_R	system heat output
Q_{trans}	heat transfer across cell (kW)
R	universal gas constant (8.314 J mol^{-1} K^{-1})
R_{ohmic}	global internal resistance (Ω m^2)
SMR	steam methane reforming reaction (R3)
T_{cell}	cell temperature (K)
U_F	fuel utilisation
WGS	water gas shift reaction (R4)
WWTP	wastewater treatment plants

Greek symbols

β	apparent charge transfer coefficient
ΔH	enthalpy change of reactions (kW)
ρ	anode material resistivity (Ω m)
δ_a	component thickness (m)
$\eta_{elec,net}$	system net electrical efficiency
η_{therm}	system thermal efficiency
$\eta_{CHP,net}$	system combined efficiency
	partial pressure of component x (bar)
ε	porosity of electrode material
τ	tortuosity of electrode porous material
γ_a	anode activation barrier overpotential coefficient (A m^{-2})
γ_c	cathode activation barrier overpotential coefficient (A m^{-2})

Subscripts

a	anode
c	cathode
e	electrode
cell	whole cell

1. Introduction

In the UK, most of the 60 million tonnes of wet sewage sludge generated at WWTPs is converted to biogas via anaerobic digestion (AD) [1]. In the majority of cases, biogas is used on site for electricity and heat production via combined heat and power (CHP) combustion engines [2]. However, with very few exceptions, the renewable electricity produced does not meet the full demand of the treatment facility. Resultantly, there has been a global research drive in recent years to decrease consumption and increase production of energy at WWTPs [3–10].

One suggested method of improving the energy balance at WWTPs is to use stationary fuel cell stacks for cogeneration in place of standard combustion-based CHP systems. High temperature fuel cells such as molten carbonate fuel cells (MCFCs) and solid oxide fuel cells (SOFCs) are the most endorsed fuel cell systems for application at WWTPs for two key reasons. Firstly, they have the ability to achieve superior electrical efficiencies to combustion-based alternatives because they are not limited by Carnot efficiency and other thermodynamic obstructions [11]. Secondly, their high temperature operation allows for internal thermo-chemical reforming capabilities and acceptance of alternative fuels such as biogas, biomethane and ammonia [12].

MCFCs, consisting of molten carbonate salt electrolytes have gained particular interest for application at WWTPs for a number of reasons. One such reason is due to the oxidation half-reaction of CO_2 at the cathode, which facilitates movement of carbonate across the electrolyte. The subsequent release of CO_2 at the anode provides the opportunity for negative emissions due to the concentration of CO_2, as long as carbon capture and utilisation or storage (CCUS) technology is employed [13,14]. It was found by Chacartegui et al. [14], that the equivalent of roughly 60% of carbon originally found in the biogas fuel generated at wastewater treatment plants could be sequestered when employing this system. However, without economic incentives to achieve negative emissions, the high costs of deployment and operation make its implementation questionable [14].

Stuttgart-Möhringen wastewater treatment plant in Germany has real operating experience with an MCFC after installation in 2007 [15]. It was found to run with a gross electrical efficiency of 44% and a net electrical efficiency of 36%. Although superior to conventional cogeneration technologies, this is inferior to the experience of SOFC devices, which classically operate with gross electrical efficiencies above 50% [12]. For example, an Italian-based project, named DEMOSOFC, plans to install a SOFC system at the SMAT Collegno WWTP in Turin [16]. A study by Mehr et al. [17] found that this plant, under nominal conditions, should run at a net electrical efficiency of 51.6%. Thus, highlighting the potential importance of the greater electrical efficiency potentials from SOFCs for WWTPs in the context of studying methods to reduce net electricity consumption. It is also the defining factor, why, this work has focussed on the incorporation of SOFCs over MCFCs at WWTPs.

Solid oxide fuel cells have historically been developed using ceramic yttria-stabilised zirconia (YSZ) electrolytes, Ni/YSZ anodes and Sr- or

Ca-doped $LaMnO_3$ cathodes which operate at temperatures between 900 and 1000 °C [18]. Over the years, efforts in material development have been made to achieve intermediate temperature (IT) SOFCS with operating temperatures in the range of 700–800 °C [19]. Lower temperatures facilitate less degradation of cell and stack components and the use of cheaper metallic interconnections over expensive lanthanum-ceramic alternatives. The research problem is overcoming the lower electrolyte conductivity, electrode kinetics and sintering temperatures of using such materials [18]. Despite the progress made in IT-SOFC development, the technology readiness levels are still markedly low [19].

Due to the R&D still ongoing with IT-SOFCs, this study has focussed on the implementation of commercially available high-temperature (HT) SOFCs, such as those resembling the Siemens-Westinghouse Power Generation Inc (SPGI) 120 kW tubular SOFC. SPGI's SOFCs are consistently referenced as model-cases for process integration studies [20–25] due to the rigorous experimental testing carried out on them, which has provided operational data for model validation and evidence of reliability and robustness [23]. High temperature operation of SOFCs also limits the degradation and poisoning caused by the presence of sulphur compounds [26], such as H_2S, which is often found in biogas.

Another important factor for UK and EU WWTPs is the limitation in the amount of ammoniacal and nitrate nitrogen that can be emitted to water-courses under the Urban Waste Water Treatment Directive (91/271/EEC) and the Water Framework Directive (2000/60/EC) [27,28]. Nitrogen control is popularly achieved via biological processing by aerobic (nitrifying) and anoxic (denitrifying) bacteria in a multi-stage activated sludge process (ASP). The nitrifying bacteria convert ammonium to nitrate whilst denitrifying bacteria convert nitrate to gaseous forms of nitrogen – i.e., mainly N_2, although N_2O is also formed. The nitrification process requires copious pumping of oxygen to the ASP and contributes largely to the total energy demand for sewage processing. It has been estimated by [29] that it takes on average 4.57 kWh of electrical energy for every kg of oxidised nitrogen.

Of chief concern are the greenhouse gas (GHG) emissions that arise from nitrogen removal during wastewater treatment. Nitrous oxide (N_2O) is generated as a metabolic intermediary and side-product during denitrification [30]. N_2O, due to its global warming potential 298 times that of CO_2 over a 100 year period, is a particularly problematic GHG [31]. There are considerable variations of GHG emissions between WWTPs, but the UK Water Industry Research Ltd (UKWIR) specify an N_2O emission factor of 0.002 kgN_2O-N emitted per 1 kg N loaded into the treatment works [32]. Thus, the diversion of nitrogenous material can have positive impacts on both energy demand and carbon footprint at WWTPs.

One key contributor of the total nitrogen load in ASP units is the liquid fraction from AD processing (digestate liquor) that returns to the head of the works. Nitrogen that is not emitted as N_2 in the ASP or discharged within the final effluent, is carried through the treatment process in sludge that is used as feedstock for onsite AD. The digestate formed during AD, therefore, contains a large quantity of nitrogen. The digestate is separated into a solid (cake) fraction and a liquid (liquor) fraction. The cake can be spread on land for nutrient reuse in agriculture, but liquor is normally recycled back into the treatment process. Problematically, the liquor retains around 70% of the total nitrogen present in the digestate [33]. It is estimated that this nitrogen equates to 15–20% of the total N-load at WWTPs [34,35].

The conditions of anaerobic digestion mean nitrogen present in the feedstock is predominantly converted to highly soluble ammonium ions (NH_4^+), hence, the reason the liquor retains more nitrogen than the solid fraction. Ammonium ions are in equilibrium with ammonia gas (NH_3) molecules as shown in (R1). Collectively known as 'total ammonia', the relative concentrations of each greatly depend on the pH of solution, where low pH conditions favour NH_4^+ and high pH conditions favour NH_3. The pH of digestate liquor normally lies between 7.5 and 8.0 which can be increased with CO_2 degassing and/or the addition of NaOH or lime [36,37]. The transformation of NH_4^+ to NH_3 then allows effective recovery of total ammonia from solution via stripping techniques. This form of ammonia recovery has been demonstrated at full scale via air stripping and absorption with [38] detailing at the time of publication, six companies providing commercially available technologies.

$$NH_3 + H_2O \rightleftarrows NH_4^+ + OH^- \quad \text{(R1)}$$

Solid oxide fuel cells have also been identified as an efficient method of using ammonia as fuel for cogeneration purposes [11,39,40]. The high temperatures used in SOFC operation facilitates the decomposition of ammonia into hydrogen and nitrogen (R5), allowing electrochemical oxidation of hydrogen and thus current generation. The work detailed in [41] has since taken this one step further by using a blend of biogas and ammonia as hydrogen carriers for use in a SOFC. An electrodeionization process was experimentally carried out to recover ammonia from synthetic ammonium-rich wastewaters for input to a three-layer button SOFC reactor with biogas produced from a lab-scale AD reactor fed with local sewage sludge. The researchers achieved 95% and 76% ammonium recovery from diluted and concentrated synthetic wastewaters respectively, and predicted a 60% improvement in net energy output compared to conventional CHP systems. However, electrodeionization has been in development for over 60 years and advancements in the fundamental understanding of its operation and application has been extremely slow [42]. Furthermore, its use often needs to be coupled with energy intensive procedures such as reverse osmosis to provide sufficient selectivity [43]. Thus, its pathway to commercialisation may still be some way off.

The aims of this study are to demonstrate the feasibility of ammonia recovery from digestate liquor via an innovative chain of practical steps, for combined use with biomethane in an internal reforming SOFC. To the knowledge of the authors of the present work, this is the first investigation of recovering ammonia for application with biomethane in a SOFC, via a sequential air-stripping and absorption. A number of steps and methods have been taken to ensure the analysis of process integration is as robust and rigorous as possible. Firstly, a WWTP operated by Yorkshire Water in the UK, has been used as a reference site for the technology application, so as to effectively determine energetic and carbon footprint implications. Aspen Plus v8.8 [44] has been used to physically model an entire optimised steady-state chemical process. A numerical modelling approach has been used to determine the electricity production and efficiency of the proposed SOFC, which corresponds and integrates with the process model.

2. Numerical fuel cell model methodology

The SOFC system modelled in this work is based on SPGI's 120 kW tubular fuel cell, as modelled for example, in [21]. It consists of three key parts; the anode, cathode and electrolyte. Methane, ammonia and steam are fed into the anode, whilst air is fed to the cathode. Oxygen molecules diffuse from the porous cathode to the cathodic triple phase boundary (TPB) where they reduce to ionic O^{2-} (R2), then through the electrolyte and on to the anodic TPB. At the anode side, three key reactions occur: (a) steam methane reforming 'SMR' (R3), (b) water gas shift 'WGS' (R4) and (c) ammonia decomposition 'NH3-DEC' (R5). Hydrogen produced diffuses through to the anodic TPB where it reacts with oxygen ions to produce steam and electrons (R6). The electrons are externally transported via a circuit to the cathode, generating electrical power.

$$0.5O_2 + 2e^- \rightarrow O^{2-} \quad \text{(R2)}$$

$$CH_4 + H_2O \rightleftarrows 3H_2 + CO \quad \text{(R3)}$$

$$CO + H_2O \rightleftarrows H_2 + CO_2 \quad \text{(R4)}$$

$$2NH_3 \rightleftarrows 3H_2 + N_2 \quad \text{(R5)}$$

$$H_2 + O^{2-} \rightarrow H_2O + 2e^- \quad \text{(R6)}$$

2.1. Cell voltage

The cell voltage is calculated by subtracting the various potential voltage losses from the Nernst Potential, shown in the following equation:

$$CV = E - n_{act} - n_{ohm} - n_{conc} \quad (1)$$

where E is the Nernst voltage potential, n_{act} represents the activation losses, n_{ohm} the ohmic losses and n_{conc} the concentration losses.

2.2. Nernst voltage potential

The Nernst Potential or the local thermodynamic reversible potential (in Equation (2)) determines the theoretical cell voltage potential under given thermodynamic conditions and compositions.

$$E = E_o - \frac{RT_{cell}}{nF}\ln\left(\frac{p_{H2O}}{p_{H2}\cdot\sqrt{p_{O2}}}\right) \quad (2)$$

where, according to [45,46]:

$$E_O = 1.2723 - (2.7645\times10^{-4} \times T_{cell} \quad (3)$$

E_o is the ideal voltage or reference voltage for hydrogen electro-chemical oxidation at ambient pressure at cell reaction sites, and a function of temperature. R is the universal gas constant, T_{cell} is absolute cell temperature, p_x is partial pressure of relevant gas species 'x', F is the Faraday constant and n is the number of electrons participating in the reaction. In this case there are two participating electrons as shown in (R6). Electrochemical oxidation of CO at the anode is neglected due to the dominance of H_2 over CO in charge transfer kinetics. Other researchers have incorporated the electrochemical oxidation of CO in numerical models, such as Spallina et al. [47]. This was found to be valid under certain conditions by experimental work carried out by Ong et al. [48], but only where high current densities (> 1.5 A cm^{-2}) and high CO concentration ($> 80\%$) conditions favoured electrochemical oxidation of CO. However, these conditions do not apply to the work presented and so it can be said with a strong degree of certainty that CO mostly contributes to the voltage potential via the production of H_2 during WGS, which also takes place at the anode (R4).

2.3. Activation voltage loss

Activation polarisation (n_{act}) is obtained via manipulation of the Butler-Volmer equation (4)

$$j = j_0\left[exp\left(\frac{\beta nFn_{act}}{RT_{cell}}\right) - exp\left(-(1-\beta)\frac{Zn\cdot n_{act}}{RT_{cell}}\right)\right] \quad (4)$$

n_{act} is determined via the Eqs. (5) and (6), extrapolated from the implicit Butler-Volmer equation and utilised by [21].

$$n_{act,a} = \frac{RT_{cell}}{\beta nF}\cdot sinh^{-1}\left(\frac{j}{2\cdot j_{0,a}}\right), \quad (5)$$

$$n_{act,c} = \frac{RT_{cell}}{\beta nF}\cdot sinh^{-1}\left(\frac{j}{2\cdot j_{0,c}}\right), \quad (6)$$

where j is the current density (A/m^2) and j_0 is the exchange current density (A/m^2). Electrodes in the anode and cathode exchange current densities, j_{0a} and j_{0c} respectively, which are determined via Eqs. (7) and (8):

$$j_{0a} = \gamma_a \times p_{H_2} \times p_{H2O} \times exp\left(\frac{-E_{aa}}{RT_{cell}}\right) \quad (7)$$

$$j_{0c} = \gamma_c \times p_{O2}^{0.25} \times exp\left(\frac{-E_{ac}}{RT_{cell}}\right) \quad (8)$$

γ_a and γ_c are activation barrier overpotential coefficients and E_{aa} *and* E_{ac} are activation energies for the anode and cathode respectively, and have each been obtained from literature. γ_a and γ_c values were taken from [21] and E_{aa} *and* E_{ac} from [49].

2.4. Ohmic voltage loss

Ohmic losses result from contact resistance, the resistance of ions moving through the electrolyte and electron transfer resistance in electrodes, current collectors and interconnects. Ohmic voltage losses have been determined using equations (9) and (10):

$$n_{ohmic} = R_{ohmic}\cdot j_{cell}\cdot A_{cell} \quad (9)$$

$$R_{ohmic} = \rho_a\delta_a + \rho_c\delta_c + \rho_e\delta_e \quad (10)$$

where A_{cell} is the area in which the current flows, R_{ohmic} is the global internal resistance which takes into account specific material resistivity (ρ) and component thickness (δ). Figures for ρ and δ have been extrapolated from [21] and subscripts a, c, and e denote the anode, cathode, and electrolyte respectively.

2.5. Concentration voltage loss

Concentration losses at electrodes occur due to mass transport processes or simplistically where fuel or oxygen is being used by the fuel cell faster than it can be supplied. The concentration losses at the cathode and anode have been calculated via the equations detailed in (11) and (12).

$$n_{conc,a} = -\frac{RT_{cell}}{n_aF}\cdot\ln\left(1 - \frac{j_{cell}}{j_{l,a}}\right) + \frac{RT_{cell}}{n_aF}\cdot\ln\left(1 + \frac{p_{H_2}j_{cell}}{p_{H_2O}J_{L,a}}\right) \quad (11)$$

$$n_{conc,c} = -\frac{RT}{n_cF}\cdot\ln\left(1 - \frac{j_{cell}}{j_{l,c}}\right) \quad (12)$$

$$j_{l,a} = \frac{2F\cdot p_{H_2}\cdot D_{a,eff}}{RT_{cell}} \quad (13)$$

$$j_{l,c} = \frac{2F\cdot p_{H_2}\cdot D_{c,eff}}{RT_{cell}} \quad (14)$$

$$D_{a,eff} = 1.3103\times10^{1.5}\cdot T_{cell}^{1.5} - 0.263382 \quad (15)$$

$$D_{c,eff} = D_{O_2}\cdot\left(\frac{T_{cell}}{273}\right)^{1.5}\cdot\frac{\varepsilon}{\tau} \quad (16)$$

where $j_{l,a}$ and $j_{l,c}$ are the anode and cathode limiting current densities respectively and $D_{a,eff}$ and $D_{c,eff}$ are effective diffusivities of H_2 and O_2 (reactant species) for the anode and cathode respectively. D_{O_2} is the ordinary diffusivity of oxygen, ε denotes porosity of the electrode and τ its tortuosity. Eq. (15) has been provided by [50], whilst (16) has been taken from [21].

2.6. Efficiency calculations

The fuel cell voltage as calculated above is based on a 120 kW SOFC using the required fixed variables from [21]. The current was calculated using the formula presented in Eq. (17). Due to the fact that each mole of oxidised hydrogen generates 2 electrons, it is derived that 0.037605 kg H_2 h^{-1} is required to generate 1 kA of current [11]. Thus, the H_2 consumption in each fuel cell was determined via Eq. (18). The fuel requirement in the cell was calculated using a fuel utilisation factor (U_F), as presented in Eq. (19). A DC/AC conversion factor of 0.97 was used to provide power outputs as AC electricity. Net power ($P_{AC,net}$) was calculated by subtracting the consumption in pumps and compressors

from the AC production. $P_{AC,net}$ was used to calculate net electrical efficiency as stated in Eq. (20) by dividing net power with LHV flows from methane and ammonia. Thermal efficiency has been calculated via Eq. (21) and combined efficiency via Eq. (22) where Q_r is the system's thermal output.

$$I_{cell} = \frac{P_{gross}}{CV} \tag{17}$$

$$\dot{m}_{H_2,consumed}(\mathrm{kg}h^{-1}) = I_{cell} \times 0.037605(\mathrm{kg}h^{-1}\mathrm{k}A^{-1}) \tag{18}$$

$$\dot{m}_{H_2,in} = \frac{\dot{m}_{H_2,consumed}}{U_F} \tag{19}$$

$$\eta_{elec,net} = \frac{P_{AC,net}}{\dot{m}_{CH_4}\cdot LHV + \dot{m}_{NH_3}\cdot LHV} \tag{20}$$

$$\eta_{therm} = \frac{Q_r}{\dot{m}_{CH_4}\cdot LHV + \dot{m}_{NH_3}\cdot LHV} \tag{21}$$

$$\eta_{CHP,net} = \frac{P_{AC,net} + Q_r}{\dot{m}_{CH_4}\cdot LHV + \dot{m}_{NH_3}\cdot LHV} \tag{22}$$

3. Simulation setup and process operation description

Aspen plus V.8.8 software [44] has been used to simulate, optimise and synergise mass and heat transfers for a combined ammonia recovery and SOFC process as if implemented at the WWTP selected as a case of study. Aspen Plus V8.8 has been used throughout with a 'COMMON' method filter and an 'NRTL-RK' base method. A short description of this method and filter and the function of blocks mentioned throughout can be found in the supplementary information provided. The following assumptions have been made:

- Ambient conditions of 1 bar and 23 °C have been used
- Air composition assumed 79:21 split of N_2:O_2 only

3.1. Fuel cell process simulation

The fuel cell modelled in Aspen Plus consists of two key parts; the anode and the cathode. The former has been represented by an RStoic block labelled 'ANODE'. Here, SMR (R3), WGS (R4), NH3-DEC (R5) and hydrogen oxidation (R6) reactions are specified along with the chosen cell temperature and pressure, as detailed in Table 5. The conversions of reactions (R3)–(R5) in the anode were determined via tests using an RGibbs reactor, which determined equilibrium via the minimisation of Gibbs free energy. An RGibbs reactor could not be used as representation of the anode due to the selectivity of electrochemical hydrogen oxidation at the triple phase boundary. Instead, an RStoic reactor was used, which defines the conversion efficiencies of CH_4, CO and NH_3 found during the above stated equilibrium investigation. Thus, the RStoic anode reactor designates 100% SMR, 52% WGS and 100% NH3-dec conversion efficiencies of CH_4, CO and NH_3 respectively. Whilst, the conversion of H_2 via (R6) corresponds to the defined fuel utilisation factor (U_F). The fuel cell exit gases are transported to a furnace, which contains unconverted hydrogen and carbon monoxide and undergo combustion.

The cathode is comprised of a 'Sep' block labelled 'CATHODE' and a 'Heater' block labelled 'FC-HEAT'. The separator allows for the flow of

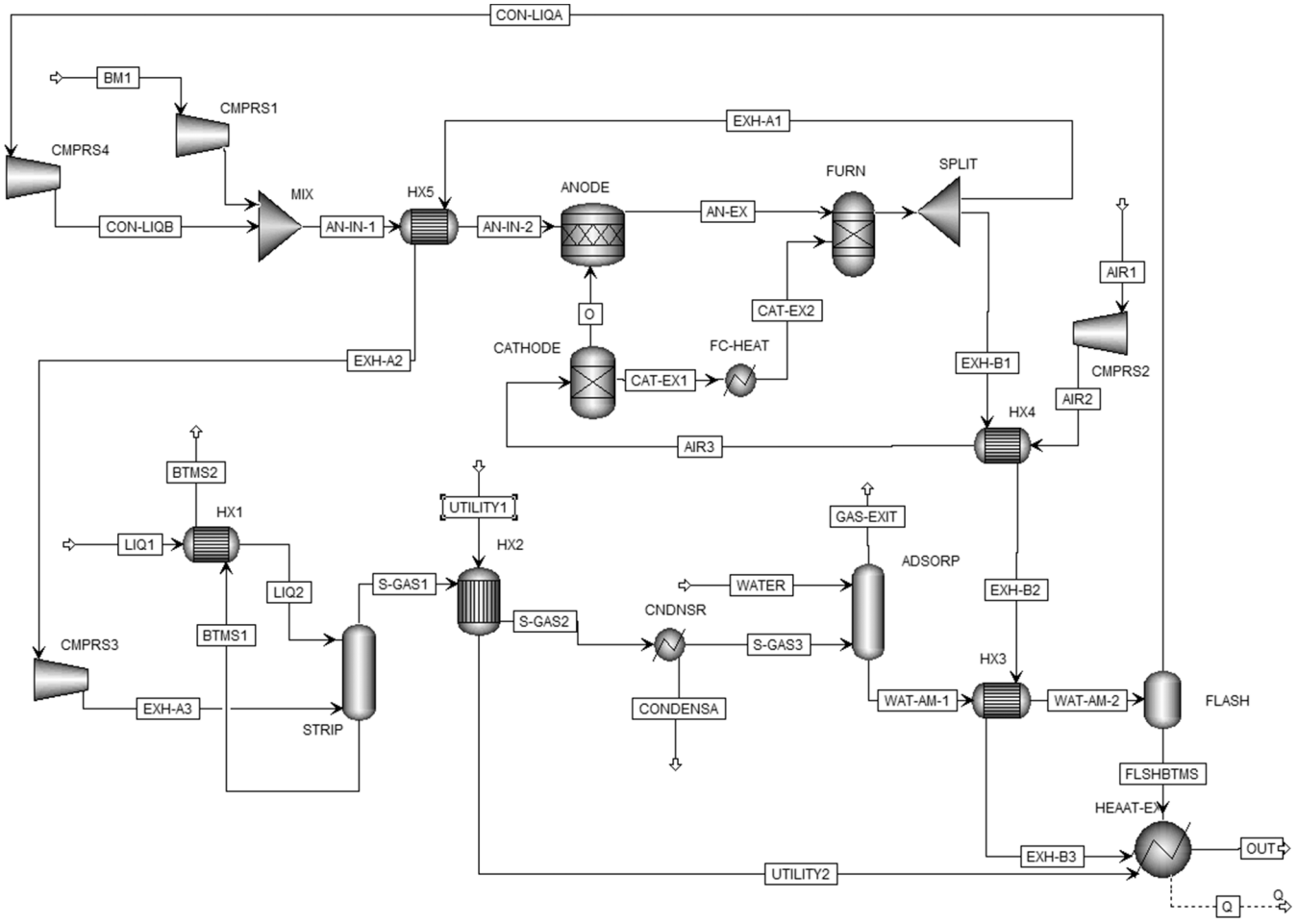

Fig. 1. Aspen Plus flow sheet of combined ammonia recovery and SOFC.

oxygen to the anode set by a 20% oxygen utilisation factor – i.e., 20% of oxygen contained in the cathode inlet is reduced and transported across the cell. The heater block 'FC-HEAT' acts purely as a representation of the heat transfer across the cell. This is required as the fuel and air inlet temperatures are below that of the SOFC operating temperature due to the combined exothermic nature of ongoing reactions. It is essential in order to fully interpret thermal properties of the system.

The heat duty or enthalpy change of reactions in the RStoic 'ANODE' is equivalent to the sum of power production ($P_{AC,net}$), heat transfer to the cathode (Q_{trans}) and any heat loss (Q_L) in the cell as shown by Eq. (23). A design specification has been installed for the simulation that varies the temperature transferred to 'AIR2′ in the heat exchanger 'HX4′ in order for Q_{trans} to fit the expression shown in Eq. (23). SOFC internal heat loss (Q_L) has been assumed at 5%.

$$-\Delta H_{an} = P_{AC,net} + Q_{trans} + Q_L \quad (23)$$

The post fuel cell furnace is simulated via an adiabatic RGibbs reactor labelled 'FURN' running at 90% thermal efficiency. The exhaust stream of which is separated via an 'FSplit' block labelled 'SPLIT'. 82% is split into the stream 'EXHAUST1′ and used for cathodic air preheating and heat transfer with the 'FLASH' inlet during ammonia recovery. The remaining 18% is used for anodic inlet pre-heating and used directly as stripping gas in the primary stage of ammonia recovery.

3.2. Ammonia recovery process simulation

The ammonia recovery part of the process model consists of three key areas; an air stripper, an absorption column and a flash drum labelled 'STRIP', 'ABSORP' AND 'FLASH' respectively. The process flow streams and units with their respective nomenclature are represented in Fig. 1. Digestate liquor is pumped into the ammonia recovery system, exchanges heat with the bottoms stream of 'STRIP' before entering the top of the column. Ammonia is being stripped in the column with 18% of the exhaust gas from the post fuel cell furnace. The exhaust gas is compressed to 1.1 bar to account for the 10% pressure drop in the 'STRIP' column. The gaseous product, exiting the top of 'STRIP', is cooled before entering at the base of the 'ABSORP' block. Here it meets a counter-current flow of water, which absorbs the ammonia, forming an aqueous product. This stream is pre-heated before entering a flash drum which vaporises a set proportion of the mixture to achieve a molar steam to carbon ratio (S:C) of 2.5 for internal SMR and WGS downstream in the SOFC.

The air stripping column (STRIP) is simulated with a RADFRAC block in Aspen plus with 30 stages, no condenser or reboiler, and functioning via equilibrium calculations. The 'LIQUOR' stream enters above stage 1 and the stripping gas enters at stage 30. A 10% pressure drop in the stripper has been assumed and implemented. The absorption column (ABSORP) is also represented by a RADFRAC block with 10 stages, without condenser or reboiler, and determined via equilibrium calculations. The stream 'WATER' enters above stage 1 and the stream 'S-GAS-2′ enters on stage 10. The flash separator (FLASH) is represented by a 'Flash2′ block with an outlet pressure of 1 bar and a vapour fraction of 0.34. Heat recovery is achieved from streams UTILITY2, EXH-B3 and FLSHBTMS. The total heat export (Q_r) is calculated via the duty of heater block HEAT-EX, which mixes UTILITY2, EXH-B3 and FLSHBTMS and cools them to ambient temperature, assuming 80% thermal efficiency.

4. Reference wastewater treatment plant conditions

A WWTP in West Yorkshire (UK) has been used as a reference treatment plant. The site treats sewage from an equivalent urban population of 750,000 people. WWTPs experience great diurnal, seasonal and spatial variability due to weather and the fluctuating nature of human activity. As such, for the benefit of analysis, average figures for parameters such as wastewater inflow, digestate production, digestate composition, electricity demand and electricity production have been used to create a steady state model.

The electricity produced at this WWTP via the biogas-CHP is documented online at [51]. The daily mean electricity production between January 2014 and December 2015 has been calculated as 40,000 kWh. However, it should be noted that WWTPs often have periods of equipment down-time where either anaerobic digesters and/or CHP equipment are out of action. The quantity of sludge-feedstock for anaerobic digestion also varies throughout the year. This brings about significant variation in biogas/electricity production. Data shows that the reference WWTP has experienced months where little or no electricity has been generated and other months where generation is 50% above the mean.

The average daily electricity demand of the facility is 60,000 kWh. It has been assumed the CHP unit at the treatment facility runs with a 35% electrical efficiency (LHV basis). Therefore, 40,000 kWh electricity would require 411,426 MJ of chemical energy which equates to 8229 kg CH_4 (based on a LHV of 50 MJ/kg). This work assumes the biogas produced onsite has been scrubbed completely of CO_2 and any impurities, such as H_2S. This generates a product of almost 100% CH_4, termed biomethane. Scrubbing the biomethane has dual benefits. Firstly, H_2S is a well-known poison to nickel catalysts and leads to increased activation polarisation losses in SOFCs [26]. Secondly, the presence of CO_2 and temporal variation of concentrations found in biogas would affect the production of hydrogen at the fuel cell's anode via equilibrium interference with WGS and SMR reactions. This, in turn, would create pronounced variation in hydrogen partial pressures and would require constant monitoring in order to effectively operate the fuel cell.

According to [52] each person in the UK generates between 133.4 L and 153.8 L of wastewater on average each day. On this basis, a figure of 140 L of wastewater generated per person per day has been assigned for the population served by the WWTP. Digestate liquor production has been inferred from [53], using an equivalent fraction of total wastewater inflow of 0.63%. Ammonia concentrations in digestate liquor were determined via analysis of 11 samples collected over a 19-month period (Oct 2015-May 2016) from the WWTP by members of the BioResource Systems Research Group and the analyses were carried out following the 4500-N Standard Method as reported in [54], at the Public Health Engineering Laboratory (School of Civil Engineering, University of Leeds).

5. Results and discussion

5.1. Ammonia recovery

Table 2 shows the mole flow data during ammonia recovery processing. The incoming liquor has an ammonia concentration of 1.8 g L^{-1} in stream 'LIQ1′ and exits at 42.8 g L^{-1} in stream 'CON-LIQA'. In total, 18% of inlet ammonia is lost in various stages of the process. This comprises of 2.7% in the air stripper, 1.7% in the absorption column and 13.6% in the flash separator. Table 2 also illustrates that 53.45 kmol h^{-1} of water is released with the recovered ammonia in stream 'CONC-LIQ'. This facilitates a downstream molar steam to carbon ratio of 2.5 and, thus, allows for effective internal SMR within the SOFC (see Table 3).

Table 1
WWTP information.

Wastewater Inflow	105,000 m^3 day^{-1}
Digestate Liquor Production	661 m^3 day^{-1}
Electricity Demand	60,000 kWh day^{-1}
Electricity produced	40,000 kWh day^{-1}
Biomethane produced	8,229 kg day^{-1}
Digestate Liquor (NH_3 –N concentration)	1.5 g L^{-1}

Table 2
Stream Results for Ammonia Recovery section of Aspen Plus Flowsheet. Flows in kmol h^{-1}, temperature (T) in °C and pressure (P) in bar. Labels as shown in Fig. 1.

	LIQ2	EXH-A3	S-gas1	S-GAS-2	WATER	WAT-AM-2	CON-LIQA
CH_4	0.00	0.00	0.00	0.00	0.00	0.00	0.00
CO	0.00	0.00	0.00	0.00	0.00	0.00	0.00
CO_2	0.00	4.08	3.96	3.96	0.00	1.28	1.28
H_2	0.00	0.00	0.00	0.00	0.00	0.00	0.00
H_2O	1528.56	17.97	87.34	87.34	170.00	164.86	53.41
N_2	0.00	114.04	113.43	113.43	0.00	0.34	0.34
NH_3	2.95	0.00	2.87	2.87	0.00	2.82	2.42
O_2	0.00	22.25	21.96	21.96	0.00	0.17	0.17
T	23.00	740.70	74.64	25.10	23.00	97.50	97.99
P	1.00	1.10	1.00	1.00	1.00	1.00	1.00

The model indicates minimal thermal losses during the three stages of ammonia recovery due to the internal heat exchange occurring in HX1 and heat recovery from streams UTILITY2, EXH-B3 and FLSHB-TMS. The overall thermal power output is calculated as 48 MWh per day. However, the combined temperature of these three streams was calculated to be 51.5 °C, indicating that the heat is of a low quality nature which has implications on its potential use in the treatment facility (as discussed later). In essence, ammonia recovery has more of an impact on the quality rather than quantity of heat available for export. The key energetic demand during ammonia recovery emanates from pre-stripping compression, which requires 1.2 MWh of electricity each day equalling 1.17 kWh/kg of recovered ammonia.

5.2. Fuel cell operation and power production

The numerical model developed in this work has been validated using experimental data from operation of SPGI's 120 kW SOFC, as shown in [55]. For the purpose of validation of the fuel cell model, a fuel inlet consisting of 89% H_2 and 11% H_2O has been used with a fuel utilisation factor of 0.85 and an operating temperature of 1000 °C. The comparative polarisation curves have been fitted with current density variation between 1000 and 4000 A m^{-2}. As illustrated in Fig. 2, there is a good match between experimental and model data. The average absolute percentage differences between model and experimental data in Fig. 2 is just 1.15%. Resultantly, it can be said with a strong degree of certainty that the fuel cell model set up for this work is representative of the application proposed here.

The combination of internal steam biomethane reforming, water gas shift and ammonia decomposition has been calculated to generate 159 kg H_2 per hour in the SOFC. Under the conditions detailed in Tables 4 and 5 using the numerical model detailed in the methodology, a cell voltage of 0.74 has been determined. The cell runs with a net electrical efficiency of 48% calculated via Equation (20). At the WWTP, this would provide 58 MWh of electricity each day and require 25 120 kW stacks in order to fulfil the power potential. The net thermal output (Q_1)

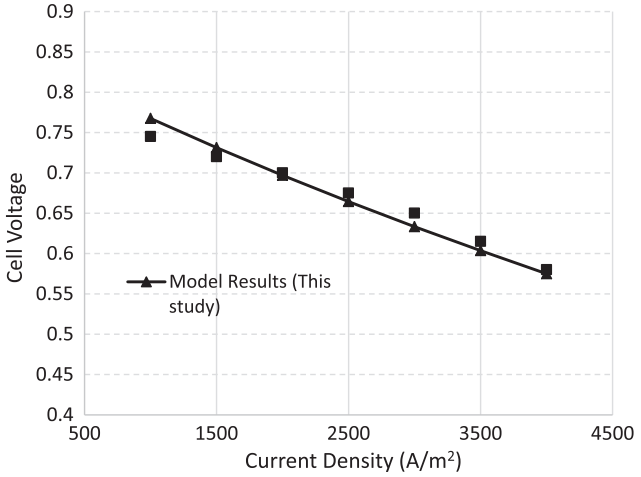

Fig. 2. Polarisation curve showing experimental data of SPGI's 120 kW SOFC from [55] and model data (from this work) using fuel composition 89% H_2 11% H_2O, U_f of 0.85 and operating temperature of 1000 °C.

Table 4
Coefficients for SOFC numerical model.

n_a		2
n_c		4
E_{aa}	J mol^{-1}	110,000
e_{ac}	J mol^{-1}	120,000
y_a	A m^{-2}	3.6×10^8
y_c	A m^{-2}	3.5×10^8
ρ_a	Ω m	2.98×10^{-5} exp (1392/T)
δ_a	m	100×10^{-6}
ρ_c	Ω m	8.114×10^{-5} exp (600/T)
δ_c	m	2.2×10^{-3}
ρ_e	Ω m	2.94×10^{-5} exp (10,350/T)
δ_e	m	40×10^{-6}
D_{O_2}	m^2 s^{-1}	4.6×10^{-2}
ε		0.39
τ		5.5

Table 5
SOFC operating conditions and results.

T_{cell}	°C	910
P_{cell}	Bar	1.08
Fuel Utilisation		0.85
Air Utilisation		0.2
Current Density	A m^{-2}	1820
Anode Inlet Temp	°C	700
Cathode Inlet Temp	°C	868
Cell Voltage	V	0.74
$\eta_{elec,net}$	%	48

Table 3
Stream Results for SOFC section of Aspen Plus Flowsheet. Flows in kmol h^{-1}, temperature (T) in °C and pressure (P) in bar. Labels as shown in Fig. 1.

	BM1	AN-IN-2	AN-EX	EXH-A1	EXH-B1	AIR3	CAT-EX1	CAT-EX2
CH_4	21.38	21.38	0.00	0.00	0.00	0.00	0.00	0.00
CO	0.00	0.00	10.26	0.00	0.00	0.00	0.00	0.00
CO_2	0.00	1.28	12.40	4.08	18.58	0.00	0.00	0.00
H_2	0.00	0.00	11.84	0.00	0.00	0.00	0.00	0.00
H_2O	0.00	53.41	87.97	17.97	81.84	0.00	0.00	0.00
N_2	0.00	0.34	1.55	114.04	519.51	632.00	632.00	632.00
NH_3	0.00	2.42	0.00	0.00	0.00	0.00	0.00	0.00
O_2	0.00	0.17	0.00	22.25	101.34	168.00	134.64	134.64
T	23.00	700.00	910.00	1075.70	1075.70	868.25	868.25	910.00
P	1.00	1.10	1.08	1.00	1.00	1.10	1.08	1.08

determined in the Aspen Plus simulation stands at 48 MWh per day. This corresponds to a thermal efficiency of 40% and a CHP efficiency of 88% as calculated via equations (21) and (22).

With the assumption that 100% of ammonia undergoes decomposition in the fuel cell, its recovery would generate an extra 176 kg H_2 each day or 4.6% of the total H_2 produced. On this basis, it can be suggested that the recovered ammonia would contribute 2.7 MWh of electricity to the facility daily. This shows that it is energetically worthwhile recovering the ammonia for use in the fuel cell with an energy balance ratio of 2.25, calculated as the ratio of electrical power produced from the ammonia in the fuel cell with the electrical energy consumed in its recovery.

Although the decomposition of ammonia has an impact on the molar production of H_2 and therefore overall power output from the stack, its effect on cell voltage is limited because the fractional molar concentration of H_2 doesn't alter significantly. For every 3 mol of H_2 generated from during ammonia decomposition (R5), 1 mol of N_2 is also generated. This helps to regulate the overall molar concentration of H_2 at the anode, which increases by just 0.8% when ammonia decomposition is taken into account. This, in turn, has a similar minimal impact on the concentration of H_2O produced by the electrochemical oxidation of H_2. As such, the introduction of recovered ammonia has a negligible effect on cell voltage and gross efficiency, but does impact significantly on the total power production of the process.

5.3. Sensitivity

Sensitivity analysis of fuel cell temperature, pressure and WGS efficiency has been carried out in order to better understand the impacts of such variables on system efficiency. Operating temperature ± 90 °C, pressure +1 bar and WGS CO conversion efficiency ± 50% have been analysed and compared to the reference model. The anode reaction efficiencies and therefore gas compositions have been assumed the same for temperature and pressure sensitivities but have been adjusted accordingly for WGS efficiency changes, including air flow for a constant oxygen utilisation of 20%.

The impact on the efficiencies η_{therm}, $\eta_{elec,net}$ and $\eta_{CHP,net}$ are displayed in Fig. 3 and Table 6. When WGS conversion efficiency is reduced, as is the hydrogen produced in the fuel cell. This limits (R6) and therefore current generation. However, the reduction in H_2 production means less air is required for pre-heating in 'HX4', allowing more heat available for export. The opposite mechanisms occur when WGS conversion efficiency is increased; contributing to greater electrochemical hydrogen oxidation and therefore power production but reduced heat generation.

Table 6
Sensitivity analysis in absolute values.

	$\eta_{elec,net}$	η_{therm}	$\eta_{CHP,net}$	CV
Reference	0.48	0.40	0.88	0.74
WGS −50%	0.46	0.42	0.87	0.73
WGS +50%	0.51	0.38	0.89	0.74
+1 bar	0.50	0.38	0.88	0.87
−90 °C	0.42	0.39	0.81	0.65
+90 °C	0.50	0.34	0.83	0.76

As shown in Table 6, when the operating pressure of the fuel cell is increased, the cell voltage also increases and therefore the current production. However, this means more heat is required in the fuel cell to allow for thermal transport. As such, more heat is exchanged with the anode inlet, reducing the final export potential by 4.6%. When combined with the increased net electricity production (which incorporates the extra energy required for compression), it gave the smallest change in combined efficiency with a 0.2% reduction.

Reducing the operating temperature of the fuel cell had the largest impact on system efficiency. Reducing the temperature negatively affects the cell voltage and therefore current and net electrical power. However, the heat loss experienced due to exchange with fuel cell inlets is significantly reduced when cell temperature is at 820 °C, resulting in appreciably more heat for export. The opposite mechanisms occur when cell operating temperature is increased by 90 °C. However, the reversed impacts on thermal and electrical efficiencies are far less substantial. This demonstrates that reducing the temperature has a far greater impact on system efficiency than increasing the temperature.

It should be noted, that with the ongoing development of IT-SOFCs operating at temperatures between 700 and 800 °C, it may be possible to achieve similar electrical efficiencies showcased in this study's reference scenario, whilst maintaining the benefits of heat export demonstrated in the above sensitivity analysis. As mentioned in the introduction, IT-SOFCs have great potential in reducing capital costs and increasing the lifetime of SOFCs. It is also expected that ammonia would still experience almost full decomposition between 700 and 800 °C; being well above required equilibrium temperatures. As such, this is highlighted as a potential avenue for future analysis and should be considered as a technological alternative once IT-SOFCs have reached a greater stage of commercialisation.

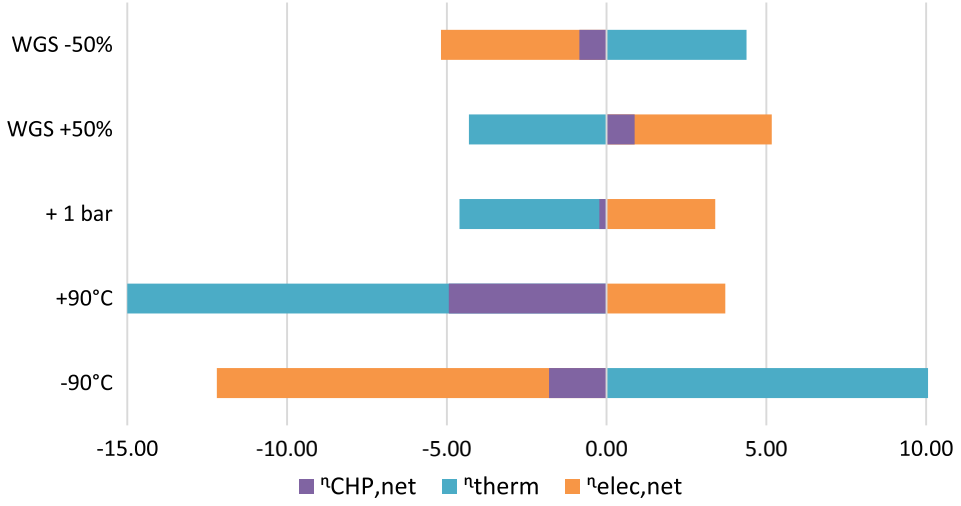

Fig. 3. Percentage impact on thermal (η_{therm}), net electrical ($\eta_{elect,\ net}$) and combined efficiency ($\eta_{CHP,\ net}$).

5.4. Impacts on wastewater treatment plant operations

Using the selected WWTP as a representative case of study of conventional sewage treatment works, the ammonia recovery process has the potential to divert up to 991 kg NH_3 daily from the activated sludge process. This would have a considerable impact on both the energy consumption and GHG emissions associated with biological nitrogen removal. Using N_2O emission factors reported by UKWIR [32], it is suggested that 1.63 kg of N_2O emissions could be avoided daily. Due to its GWP being 298 times over a 100-year period, this equates to 486 kg CO_2e of daily avoidance. However, N_2O emissions from biological N-removal are a notoriously difficult parameter to predict. For example, [30] found emission factors varying between 0 and 14.6% of nitrogen load, with most cases showing greater emissions than that suggested by UKWIR. This implies that GHG emission savings could be far greater than those presented in this work.

Considering the average electricity demand at this WWTP stands at around 60 MWh each day (Table 1), considerable energy savings can be expected if the discussed process is implemented. The diversion of ammonia from conventional treatment mitigates the use of almost 3.7 MWh (6%) of electricity daily due to the decreased aeration required for N-removal in the activated sludge process. Furthermore, the use of the proposed system means the daily power generated could alter from 40 MWh a day to 58 MWh; a 45% increase. Thus, under nominal loads the plant would transition from a net consumer of 20 MWh of centrally generated electricity daily (and its associated losses through grid transmission) to a net local generator of 1.7 MWh daily; making the plant 100% electricity self-sufficient.

It was mentioned in Section 6 that the WWTP experiences significant variation in the production of bio-methane depending on AD performance. This is important as it will vary the overall power-output of the process. However, as long as the feed molar steam to carbon ratio of the system is kept constant at 2.5, fuel utilisation factor is kept constant at 0.85 and the air utilisation factor is kept constant at 0.2, then the overall efficiency of the operation can be kept fairly consistent. Unfortunately, control strategies for dynamic operation of SOFCs come with their own set of issues, which are well reviewed in articles such D'Andrea et al. [56] and Jiang et al. [57]. With this in mind, it may be important for WWTP operators to effectively manage the storage of biogas/biomethane so that throughput to the SOFC can be kept as constant as possible.

These projections mean the consumption of 20 MWh per day of grid electricity can be omitted at this WWTP. This has the potential to save both considerable operating costs and life cycle GHG emissions. Using a 10.5 pence per kW electricity purchasing price [58], it would save the facility £766,500 a year in power costs. Meanwhile, the lifecycle emission intensity of UK electricity currently stands at 107 gCO_2e/kWh [59]. At this WWTP, that would equate to 2140 kg CO_2e of reduced GHG emissions each day due to mitigated grid electricity use. On top of the 486 kg CO_2e savings facilitated by ammonia diversion, a total of 2626 kg CO_2e lifecycle emission savings could be made daily. This equates to 3.5 kg CO_2e PE^{-1} $year^{-1}$.

The 48 MWh per day of thermal power generated from the system is expected to be enough to meet the demands of the facility where heat is used for activities such as, anaerobic digestion, space heat and sludge drying. However, its low quality nature of 51.5 °C at 1 bar may limit its application potential in plants where high quality heat is required. In such cases, excess electrical power could be used to upgrade the heat. Heat utilisation and upgrading is an area where further and future work is suggested.

As mentioned in the introduction, the system described in [41] also acts to recover ammonia from digestate liquor for combined use with biogas. The ammonia recovery efficiency using an electrodeionization set-up lies between 76 and 95% depending on the concentration of solution, thus, comparable to the efficiency found in this paper's work of 82%. However, [41] reported that the electrodeionization unit ran with energy balance ratios between 0.5 and 1.2 during batch experiments. In this sense, the ammonia recovery modelled in this paper via stripping and absorption is energetically superior with an energy balance ratio of 2.25.

6. Conclusions

In this work, a novel system of ammonia recovery for combined use alongside biomethane in a SOFC has been developed for application at WWTPs. The entire process has been modelled and optimised using Aspen Plus (V.8.8) and examined numerically, demonstrating its technical feasibility and potential impact on the two primary sustainability issues for WWTPs; net energy use and greenhouse gas emissions.

The analysis has shown implementation of this technology could have significant impacts on the environmental and energetic sustainability of wastewater treatment plants around the world, as most modern WWTPs using nitrification/denitrification and anaerobic digestion technology do not meet their own energetic needs with conventional CHP units. The modelling from this paper indicates an increase in renewable electricity production by 45% and a reduction in consumption of 6% is achievable. Thus, from an energetic point of view, this technology would be extremely attractive to treatment facilities, whose current treatment process is similar to our case of study. In the UK, it would mean that average energy consumption for sewage treatment could be reduced from 80 to 75 Wh per person per day (saving 325 MWh daily for the entire country), with a substantial increment of onsite energy generation into the net energy consumption – i.e., from 66% contribution via conventional AD-CHP units to 102% contribution via the proposed system.

Furthermore, analysis in this work demonstrates that an annual reduction in GHG emissions of 3.4 kg CO_2e per person served by a WWTP is achievable. If large-scale implementation of this process was carried out, it could have significant impact on the global effort to tackle climate change. Moreover, reducing GHG emissions could play a key role in the financial viability of this technology, if carbon taxes or similar carbon reduction incentives are integrated into worldwide economies in the future.

Importantly, this technology is not limited to use only at wastewater treatment plants. The process is essentially an addition to conventional anaerobic digestion and could be implemented accordingly. Simulations show the potential to recover over 80% of ammoniacal nitrogen present in digestate liquor, which if used in integrated SOFC stacks with biomethane, significantly boosts electrical power potential. Thus, if this process was rigged alongside other AD plants it could play an important part in the global integration of renewables and the environmental sustainability of industries that utilise AD.

Acknowledgments

The authors would like to thank the UK's Engineering and Physical Sciences Research Council's (EPSRC) Centre for Doctoral Training on Bioenergy (EP/L014912/1) for the financial support of Mr. Oliver Grasham with his PhD Scholarship. Further recognition to the EPSRC for their grant award NWaste2H2 EP/R00076X/1. The authors' gratitude also extends to Yorkshire Water for allowing access to one of their WWTPs for the collection of samples.

Appendix A

See Table A1.

Table A1
Aspen Plus blocks and property method descriptions.

RGibbs	Reactor block that calculates output composition based on the minimisation of Gibbs free energy under set conditions
RStoic	Reactor block that calculates output composition based on specified molar conversions of stated reactions
Mixer	Combines multiple material, heat or work streams to an individual outlet
Sep	Separates individual components of a stream or streams by specified fractions or quantities
Flash2	Capable of simulating flashes, evaporators, knock-out drums. Calculates thermal and phase conditions for vapour-liquid separation
FSplit	Separates material, heat or work streams into two or more according to specified splits. All outlet streams contain the same fractional composition.
Compr	Simulates both compressors and turbines. In this work both compressors and turbines have been modelled as isentropic. Performs power consumption or production calculations based on desired pressure outlet.
Pump	Models pumps or hydraulic turbines. Designed to handles single-liquid phase inlet streams. Performs power consumption or production calculations based on desired pressure outlet.
HeatX	Capable of simulating a variety of heat exchangers. In this work 'shortcut' option has been used with counter-current flow. Calculates heat transfer capabilities based on properties of hot and cold side flows.
Heater	Capable of simulating heaters and coolers. Calculates thermal and phase conditions for one or more inlet streams under specified conditions (normally temperature and pressure).
RadFrac	Capable of modelling all types of multistage vapour-liquid fractionation operations including stripping and absorption
NRTL-RK Property Method	Component properties are based on NRTL activity coefficient model for liquid phase, Redlich-Kwong equation of state for vapour phase, Rackett model for liquid molar volume and Henry's law for supercritical components

Appendix B. Supplementary material

Supplementary data to this article can be found online at https://doi.org/10.1016/j.apenergy.2019.02.029.

References

[1] Zhang Q, Hu J, Lee DJ, Chang Y, Lee YJ. Sludge treatment: Current research trends. Bioresour Technol 2017;243:1159–72. https://doi.org/10.1016/j.biortech.2017.07.070.
[2] ADBA. Anaerobic Digestion Market report July 2015; 2015.
[3] Guest JS, Skerlos SJ, Barnard JL, Beck MB, Daigger GT, Hilger H, et al. A new planning and design paradigm to achieve sustainable resource recovery from wastewater. Environ Sci Technol 2009;43:6126–30. https://doi.org/10.1021/es9010515.
[4] McCarty PL, Bae J, Kim J. Domestic wastewater treatment as a net energy producer - can this be achieved? Environ Sci Technol 2011;45:7100–6. https://doi.org/10.1021/es2014264.
[5] Chudoba P, Sardet C, Palko G, Guibelin E. Main factors influencing anaerobic digestion of sludge and energy efficiency at several large WWTP in central Europe. J Residuals Sci Technol 2011;8:89–96.
[6] Larsen TA, Alder AC, Eggen RIL, Maurer M, Lienert J. Source separation: will we see a paradigm shift in wastewater handling? Environ Sci Technol 2009;43:6121–5. https://doi.org/10.1021/es803001r.
[7] Silva C, Rosa MJ. Energy performance indicators of wastewater treatment: a field study with 17 Portuguese plants. Water Sci Technol 2015;72:510–9. https://doi.org/10.2166/wst.2015.189.
[8] Schaubroeck T, De Clippeleir H, Weissenbacher N, Dewulf J, Boeckx P, Vlaeminck SE, et al. Environmental sustainability of an energy self-sufficient sewage treatment plant: improvements through DEMON and co-digestion. Water Res 2015;74:166–79. https://doi.org/10.1016/j.watres.2015.02.013.
[9] Siegrist H, Salzgeber D, Eugster J, Joss A. Anammox brings WWTP closer to energy autarky due to increased biogas production and reduced aeration energy for N-removal; 2008.
[10] WERF. Energy Management Exploratory Team Report Executive Summary; 2011.
[11] EG&G Technical Services I. Fuel Cell Handbook. Fuel Cell 2004;7 Edition:1–352. https://doi.org/10.1002/zaac.200300050.
[12] Hajimolana SA, Hussain MA, Daud WMAW, Soroush M, Shamiri A. Mathematical modeling of solid oxide fuel cells: a review. Renew Sustain Energy Rev 2011;15:1893–917. https://doi.org/10.1016/j.rser.2010.12.011.
[13] Amorelli A, Wilkinson MB, Bedont P, Capobianco P, Marcenaro B, Parodi F, et al. An experimental investigation into the use of molten carbonate fuel cells to capture CO2 from gas turbine exhaust gases. Energy 2004;29:1279–84. https://doi.org/10.1016/j.energy.2004.03.087.
[14] Chacartegui R, Monje B, Sanchez D, Becerra JA, Campanari S. Molten carbonate fuel cell: towards negative emissions in wastewater treatment CHP plants. Int J Greenh Gas Control 2013;19:453–61. https://doi.org/10.1016/j.ijggc.2013.10.007.
[15] Locher C, Meyer C, Steinmetz H. Operating experiences with a molten carbonate fuel cell at Stuttgart-Möhringen wastewater treatment plant. Water Sci Technol 2012;65:789–94. https://doi.org/10.2166/wst.2012.463.
[16] DEMOSOFC. DEMOSOFC FCH2-JU PROJECT 2018. http://www.demosofc.eu/ [accessed October 23, 2018].
[17] Mehr AS, Gandiglio M, MosayebNezhad M, Lanzini A, Mahmoudi SMS, Yari M, et al. Solar-assisted integrated biogas solid oxide fuel cell (SOFC) installation in wastewater treatment plant: energy and economic analysis. Appl Energy 2017;191:620–38. https://doi.org/10.1016/j.apenergy.2017.01.070.
[18] Singhal SC. Solid oxide fuel cells for stationary, mobile, and military applications. Solid State Ionics 2002;152–153:405–10. https://doi.org/10.1016/S0167-2738(02)00349-1.
[19] Krishnan VV. Recent developments in metal-supported solid oxide fuel cells. Wiley Interdiscip Rev Energy Environ 2017;6. https://doi.org/10.1002/wene.246.
[20] Bharadwaj A, Archer DH, Rubin ES. Modeling the performance of a tubular solid oxide fuel cell. J Fuel Cell Sci Technol 2005;2:38. https://doi.org/10.1115/1.1842781.
[21] Minutillo M, Perna A, Jannelli E. SOFC and MCFC system level modeling for hybrid plants performance prediction. Int J Hydrogen Energy 2014;39:21688–99. https://doi.org/10.1016/j.ijhydene.2014.09.082.
[22] Doherty W, Reynolds A, Kennedy D. Process simulation of biomass gasification integrated with a solid oxide fuel cell stack. J Power Sources 2015;277:292–303. https://doi.org/10.1016/j.jpowsour.2014.11.125.
[23] Bao C, Wang Y, Feng D, Jiang Z, Zhang X. Macroscopic modeling of solid oxide fuel cell (SOFC) and model-based control of SOFC and gas turbine hybrid system. Prog Energy Combust Sci 2018;66:83–140. https://doi.org/10.1016/j.pecs.2017.12.002.
[24] Zhang W, Croiset E, Douglas PL, Fowler MW, Entchev E. Simulation of a tubular solid oxide fuel cell stack using AspenPlus™ unit operation models. Energy Convers Manag 2005;46:181–96. https://doi.org/10.1016/j.enconman.2004.03.002.
[25] Ameri M, Mohammadi R. Simulation of an atmospheric SOFC and gas turbine hybrid system using Aspen Plus software. Int J Energy Res 2013;37:412–25. https://doi.org/10.1002/er.
[26] Nagel FP, Schildhauer TJ, Sfeir J, Schuler A, Biollaz SMA. The impact of sulfur on the performance of a solid oxide fuel cell (SOFC) system operated with hydrocarboneous fuel gas. J Power Sources 2009;189:1127–31. https://doi.org/10.1016/j.jpowsour.2008.12.092.
[27] CEC – Council of the European Communities. Directive concerning urban waste water treatment (91/271/EEC). Off J Eur Communities 1991;L135:40–52 (30 May).
[28] CEC – Council of the European Communities. Directive establishing a framework for Community action in the field of water policy (2000/60/EC). Off J Eur Communities 2000;L327:1–72 (22 December).
[29] Garrido JM, Fdz-Polanco M, Fdz-Polanco F. Working with energy and mass balances: a conceptual framework to understand the limits of municipal wastewater treatment. Water Sci Technol 2013;67:2294. https://doi.org/10.2166/wst.2013.124.
[30] Kampschreur MJ, Temmink H, Kleerebezem R, Jetten MSM, van Loosdrecht MCM. Nitrous oxide emission during wastewater treatment. Water Res 2009;43:4093–103. https://doi.org/10.1016/j.watres.2009.03.001.
[31] IPCC IPOCC. Climate Change 2007 - The Physical Science Basis: Working Group I Contribution to the Fourth Assessment Report of the IPCC. Science (80-) 2007:1009.
[32] Andrews J, Chambers B, Davey A, Galetti S, Hobson J, Hunt D, et al. Carbon accounting in the water industry; non-co2 emissions. London: UKWIR; 2009.
[33] Bauer A, Mayr H, Hopfner-Sixt K, Amon T. Detailed monitoring of two biogas plants and mechanical solid–liquid separation of fermentation residues. J Biotechnol 2009;142:56–63. https://doi.org/10.1016/j.jbiotec.2009.01.016.

[34] Maurer M, Schwegler P, Larsen T. Nutrients in urine: energetic aspects of removal and recovery. Water Sci Technol 2003;48:37–46.
[35] Fux C, Siegrist H. Nitrogen removal from sludge digester liquids by nitrification/denitrification or partial nitritation/anammox: environmental and economical considerations. Water Sci Technol 2004;50:19–26.
[36] Guštin S, Marinšek-Logar R. Effect of pH, temperature and air flow rate on the continuous ammonia stripping of the anaerobic digestion effluent. Process Saf Environ Prot 2011;89:61–6. https://doi.org/10.1016/j.psep.2010.11.001.
[37] Drosg B, Fuchs W, Al Seadi T, Madsen M, Linke B. Nutrient recovery by biogas digestate processing. IEA Bioenergy; 2015.
[38] Vaneeckhaute C, Lebuf V, Michels E, Belia E, Vanrolleghem PA, Tack FMG, et al. Nutrient recovery from digestate: systematic technology review and product classification. Waste Biomass Valoriz 2016:1–20. https://doi.org/10.1007/s12649-016-9642-x.
[39] Borello D, Del Prete Z, Marchegiani A, Rispoli F, Tortora E. Analysis of an integrated PEMFC/ORC power system using ammonia for hydrogen storage, vol. 3 Cycle Innov Educ Electr Power; Fans Blowers; Ind Cogener 2012;3:143. https://doi.org/10.1115/GT2012-68599.
[40] Ni M, Leung DYC, Leung MKH. Mathematical modeling of ammonia-fed solid oxide fuel cells with different electrolytes. Int J Hydrogen Energy 2008;33:5765–72. https://doi.org/10.1016/j.ijhydene.2008.07.021.
[41] Xu L, Dong F, Zhuang H, He W, Ni M, Feng SP, et al. Energy upcycle in anaerobic treatment: ammonium, methane, and carbon dioxide reformation through a hybrid electrodeionization–solid oxide fuel cell system. Energy Convers Manag 2017;140:157–66. https://doi.org/10.1016/j.enconman.2017.02.072.
[42] Alvarado L, Chen A. Electrodeionization: principles, strategies and applications. Electrochim Acta 2014;132:583–97. https://doi.org/10.1016/j.electacta.2014.03.165.
[43] Mondor M, Masse L, Ippersiel D, Lamarche F, Massé DI. Use of electrodialysis and reverse osmosis for the recovery and concentration of ammonia from swine manure. Bioresour Technol 2008;99:7363–8. https://doi.org/10.1016/j.biortech.2006.12.039.
[44] Aspen Plus. Aspen Technology. Inc, Version, 88; 2015.
[45] Campanari S, Iora P. Definition and sensitivity analysis of a finite volume SOFC model for a tubular cell geometry. J Power Sources 2004;132:113–26. https://doi.org/10.1016/j.jpowsour.2004.01.043.
[46] Lisbona P, Corradetti A, Bove R, Lunghi P. Analysis of a solid oxide fuel cell system for combined heat and power applications under non-nominal conditions. Electrochim Acta 2007;53:1920–30. https://doi.org/10.1016/j.electacta.2007.08.046.
[47] Spallina V, Mastropasqua L, Iora P, Romano MC, Campanari S. Assessment of finite volume modeling approaches for intermediate temperature Solid Oxide Fuel Cells working with CO-rich syngas fuels. Int J Hydrogen Energy 2015;40:15012–31. https://doi.org/10.1016/j.ijhydene.2015.08.101.
[48] Ong KM, Lee WY, Hanna J, Ghoniem AF. Isolating the impact of CO concentration in syngas mixtures on SOFC performance via internal reforming and direct oxidation. Int J Hydrogen Energy 2016;41:9035–47. https://doi.org/10.1016/j.ijhydene.2016.03.107.
[49] Nagel FP, Schildhauer TJ, Biollaz SMA. Biomass-integrated gasification fuel cell systems - Part 1: Definition of systems and technical analysis. Int J Hydrogen Energy 2009;34:6809–25. https://doi.org/10.1016/j.ijhydene.2009.05.125.
[50] Lee TS, Chung JN, Chen YC. Design and optimization of a combined fuel reforming and solid oxide fuel cell system with anode off-gas recycling. Energy Convers Manag 2011;52:3214–26. https://doi.org/10.1016/j.enconman.2011.05.009.
[51] Variable Pitch. Details of Esholt STW CHP 2017. http://www.variablepitch.co.uk/stations/748/ [accessed March 9, 2017].
[52] Ofwat. Security of supply 2006-07 report; 2007.
[53] Mininni G, Laera G, Bertanza G, Canato M, Sbrilli A. Mass and energy balances of sludge processing in reference and upgraded wastewater treatment plants. Environ Sci Pollut Res Int 2015;22:7203–15. https://doi.org/10.1007/s11356-014-4013-2.
[54] AWWA. 4500-NH3 F. Stand. methods Exam. water wastewater; 1999.
[55] Williams MC, Strarkey JP, Singhal SC. US distributed generation fuel cell program. In: Brandon N, Thompsett D, editors. Fuel cells compend. 1st ed.Oxford, UK: Elsevier Ltd; 2005. p. 4.
[56] D'Andrea G, Gandiglio M, Lanzini A, Santarelli M. Dynamic model with experimental validation of a biogas-fed SOFC plant. Energy Convers Manag 2017;135:21–34. https://doi.org/10.1016/j.enconman.2016.12.063.
[57] Jiang W, Fang R, Khan J, Dougal R. Control strategies for start-up and part-load operation of solid oxide fuel cell/gas turbine hybrid system. J Fuel Cell Sci Technol 2010;7:110161–9. https://doi.org/10.1115/1.3006197.
[58] BEIS, Department for Business E& IS. Prices of fuels purchased by non-domestic consumers in the UK. Quaterly Energy Prices; 2017.
[59] BEIS, Department for Business E& IS. Updated Energy and Emissions Projections 2017; 2018.